

Article

Effect of Electron Correlations on the Electronic Structure and Magnetic Properties of the Full Heusler Alloy Mn_2NiAl

Evgeniy D. Chernov^{1,*}  and Alexey V. Lukoyanov^{1,2} 

¹ M.N. Mikheev Institute of Metal Physics, Ural Branch, Russian Academy of Sciences, S. Kovalevskaya Str., 18, 620108 Ekaterinburg, Russia

² Institute of Physics and Technology, Ural Federal University, Mira Str., 21, 620002 Ekaterinburg, Russia; lukoyanov@imp.uran.ru

* Correspondence: chernov_ed@imp.uran.ru; Tel.: +7-343-378-3886

Abstract: In this theoretical study, we investigate the effect of electron correlations on the electronic structure and magnetic properties of the full Heusler alloy Mn_2NiAl in the framework of first-principles calculations. We investigate the electron correlation effect as employed within hybrid functional (HSE) and also within the DFT+U method with varied values of parameters between 0.9 and 6 eV. The XA-crystal structure was investigated with antiferromagnetic orderings of the magnetic moments of the manganese. It was found that with a growth of the Coulomb interaction parameter, the manganese ions magnetic moment increases, and it reaches the value of 4.15–4.46 μ_B per Mn. In addition, the total magnetic moment decreases because of the AFM ordering of the Mn ions and a small magnetic moment of Ni. The calculated total magnetic value agrees well with recent experiments demonstrating a low value of magnetization. This experimental value is most closely reproduced for the moderate values of the Coulomb parameter, also calculated in constrained LDA, while previous DFT studies substantially overestimated this value. It is also worth noticing that for all values of the Coulomb interaction parameter, this compound remains metallic in its electronic structure in agreement with transport measurements.

Keywords: electronic structure; Heusler alloys; magnetic moments; electron correlations; DFT



Citation: Chernov, E.D.; Lukoyanov, A.V. Effect of Electron Correlations on the Electronic Structure and Magnetic Properties of the Full Heusler Alloy Mn_2NiAl . *Magnetochemistry* **2023**, *9*, 185. <https://doi.org/10.3390/magnetochemistry9070185>

Academic Editors: Tingping Hou and Evangelos Hristoforou

Received: 30 April 2023

Revised: 4 July 2023

Accepted: 11 July 2023

Published: 17 July 2023



Copyright: © 2023 by the authors. Licensee MDPI, Basel, Switzerland. This article is an open access article distributed under the terms and conditions of the Creative Commons Attribution (CC BY) license (<https://creativecommons.org/licenses/by/4.0/>).

1. Introduction

Heusler alloys belong to a wide family of materials, which can be metals, semiconductors, superconductors, topological insulators, or other classes of compounds [1]. Discovery of novel Heusler alloys is supported by theoretical modeling [2,3]. Heusler alloys have gained significant attention in recent years due to their remarkable properties, including high-temperature stability, half-metallicity, and ferromagnetic shape-memory behavior, and they can be used as functional materials in spin-dependent devices, etc. [4,5]. Among the various Heusler alloys, the Mn-based Heusler alloys have been extensively studied due to their potential applications in spintronics and magnetic storage devices [6]. In a number of theoretical papers, it was shown that the local spin density approximation (LSDA) or GGA schemes are not sufficient for describing the electronic structure correctly [7]. For transition-metal-based half-metallic compounds, the calculated Hubbard U parameters lie between 1.7 and 3.8 eV, being the smallest for MnAs (Mn-3d orbitals) [8] and largest for Cr_2CoGa (Co-3d orbitals) [9]. However, Mn-based full Heusler compounds such as Co_2MnSi lose their half-metallic behavior if the correlation becomes too strong (above 2 eV) [10]. A recent study showed that values of Hubbard U and Hund exchange J parameters for Mn ions vary between 0.55 (0.44) eV and 2.60 (0.83) eV [11]. In particular, in Mn2-based alloys, two ferromagnetic alloys, Mn_2NiGa and Mn_2NiSn , were found with shape memory properties and Curie temperature values equal to 588 K [12] and 530 K [13], respectively. Mn_2NbAl and Mn_2NiGe were theoretically calculated as half-metallic alloys [14,15]. However, these alloys based on Mn2 in many studies were found in a complicated β -Mn structure [8,16] or

even in the hexagonal structure in the case of Mn_2PtAl [6]. Mn_2NiAl is a prototype Mn-based Heusler alloy that exhibits interesting electronic and magnetic properties, making it a promising material for various applications. The electronic structure of Mn_2NiAl was studied by first-principles calculations [17,18], and Mn_2NiAl was found to be a ferrimagnet with the total magnetic moments of 1.48 and 1.14 μ_B /f.u. for the austenite and the martensite, respectively. The total moment was estimated to be formed by the antiparallel aligned Mn moments and a small contribution of Ni moment [17,18], which was confirmed by recent experimental studies for Mn_2NiAl and $\text{Mn}_{50}\text{Ni}_{50-x}\text{Al}_x$ ribbons [19] and Monte Carlo simulations [15]. An experimental study [20] revealed that Mn_2NiAl has the inverse Xa-type structure and anomalies in the temperature dependence of the magnetization, which correlate with the electrical resistivity anomalies [20]. The experimental magnetization of Mn_2NiAl was found to be as low as 0.2 μ_B [20]; however, theoretical studies substantially overestimate this small experimental value of magnetization of the studied alloy.

In order to understand why Mn_2NiAl has such a small magnetization, in this work we evaluate the electron correlations and determine their effect on the electronic and magnetic structure of the compound under study. Our work sheds light on the role of electron correlations in determining the electronic and magnetic properties of Mn_2NiAl . The results of our study will be useful for designing Mn-based Heusler alloys with desired properties for various applications in spintronics and magnetic storage devices.

2. Materials and Methods

The Mn_2NiAl full Heusler alloy has a cubic $F\bar{4}3m$ structure of symmetry group number 216 in the list of crystallographic groups, with unit cell parameters: $a = b = c = 5.795 \text{ \AA}$, $\alpha = \beta = \gamma = 90^\circ$. As shown in Figure 1, the alloy forms the Xa-type inverse Heusler structure. Atomic positions are Mn1 (0, 0, 0), Mn2 (0.25, 0.25, 0.25), Ni (0.5, 0.5, 0.5), and Al (−0.25, −0.25, −0.25). The Mn atoms are indicated in purple, Ni atoms—gray, and Al atoms—blue. The unit cell of the Mn_2NiAl contains two manganese atoms, one nickel atom, and one aluminum atom. The manganese ions Mn1 and Mn2 are in the antiparallel alignment. The crystal structure of Mn_2NiAl is plotted in Vesta [21].

In this work, the electronic structure of the Mn_2NiAl alloy was computed using the Quantum ESPRESSO software package [22]. This software package contains the most common basic and advanced exchange–correlation approximations and methods, as well as an impressive set of post-processing tools. The exchange–correlation potential was employed in a generalized gradient approximation (GGA) of Perdew–Burke–Ernzerhof (PBE) type [23]. To take into account electron correlations, the DFT+U method [24] was used with $U_{eff} = U - J$, with the values of Coulomb parameter in the range between 0.9 and 6 eV, and the calculated values for Mn^{2+} ions. The Coulomb interaction is not considered for Ni ions. The DFT+U method is an extension of the density functional theory (DFT) that is used to improve the description of strongly correlated electronic systems. In standard DFT, the exchange–correlation functional is approximated as a local density approximation (LDA) or GGA, which can lead to inaccuracies in the description of localized electronic states and strong electron–electron interactions. In turn, the DFT+U method introduces a Hubbard-like term, to the Hamiltonian that describes the onsite Coulomb repulsion U , between electrons in localized orbitals. To calculate the Coulomb interaction parameter for Mn atoms (3d shell), we use constrained DFT calculations in the form of a linear response to a certain potential applied to the system. In order to evaluate the effect of electronic correlations, we make a series of calculations varying the value of the Coulomb interaction parameter in the range from 0.9 to 6 eV. An alternative approach to take into account electron correlations was also used, namely, the hybrid functional HSE. The hybrid functional HSE (Heyd–Scuseria–Ernzerhof) is a density functional theory method that combines the traditional exchange–correlation functionals with a fraction of Hartree–Fock (HF) exchange. In the HSE method, the exchange–correlation functional is split into two parts: a short-range part that is described by LDA or GGA, and a long-range part that is described by a fraction of HF exchange. The weight of the HF exchange is

determined empirically or from *ab initio* calculations. In our calculations, for the correct estimation of the Coulomb interaction parameter, we use the weight of the HF exchange equal to the standard value of 0.3. K-grid and q-grid dimensions consist of $4 \times 4 \times 4$ points. For GGA and DFT+U calculation, the k-grid dimension consists of $8 \times 8 \times 8$ points. The calculations used the standard ultrasoft potentials from the pseudopotential library of Quantum ESPRESSO [25].

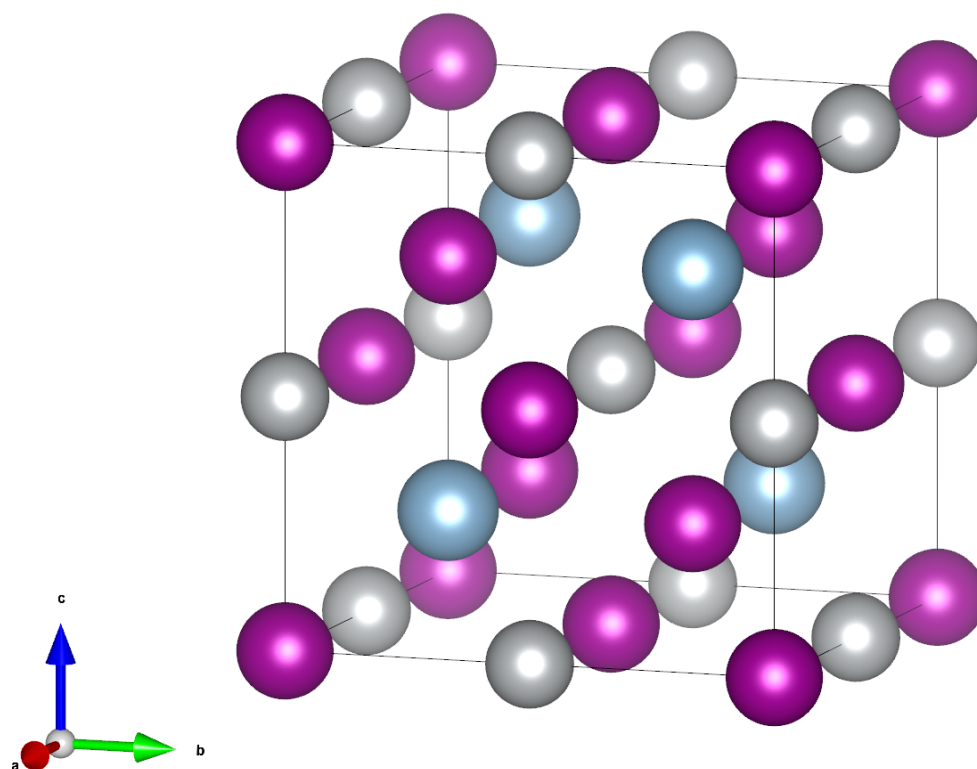


Figure 1. The crystal structure of Mn_2NiAl . The Mn atoms are indicated in purple, Ni atoms—gray, and Al atoms—blue.

3. Results and Discussions

It is worth noting that the studies were carried out as in the case of the initial ferromagnetic or antiferromagnetic ordering of manganese atoms. In the course of self-consistent calculations, it was found that all starting orderings converged to the ferrimagnetic one. Thus, the antiparallel alignment of the Mn ions was found to be energetically favorable. Therefore, below, we consider it.

In our investigation, the GGA calculation for experimental lattice parameter value 5.795 \AA (Figure 2) was performed first. As can be seen, Mn_2NiAl exhibits semimetallic properties in the “minority” spin projection and metallic properties in the “majority” spin projection. Let us consider this in detail (Figure 3). In the “minority” spin projection, indirect bandgaps are observed in the vicinity of the Fermi energy. The Mn band intersects the Fermi energy in the conduction band, but no bands from the valence band cross it. In the energy range between -4 and -1 eV, the strong hybridization between the Mn and Ni electronic states with the high peaks in the density of states is observed. In the case of the “minority” spin projection, the hybridization between the Mn and Ni states with the high peaks of the density of states is observed too. Mostly, this hybridization and peaks are observed in the valence band, but in the conduction band the narrow peaks of the Mn 3d states are observed at 1.3 eV in the “majority” spin projection and near 0.8 eV. It is important to note that the densities of electronic states for different spin projections differ from each other and are not mirrored. Based on this, it can be concluded that Mn_2NiAl is a ferrimagnetic material.

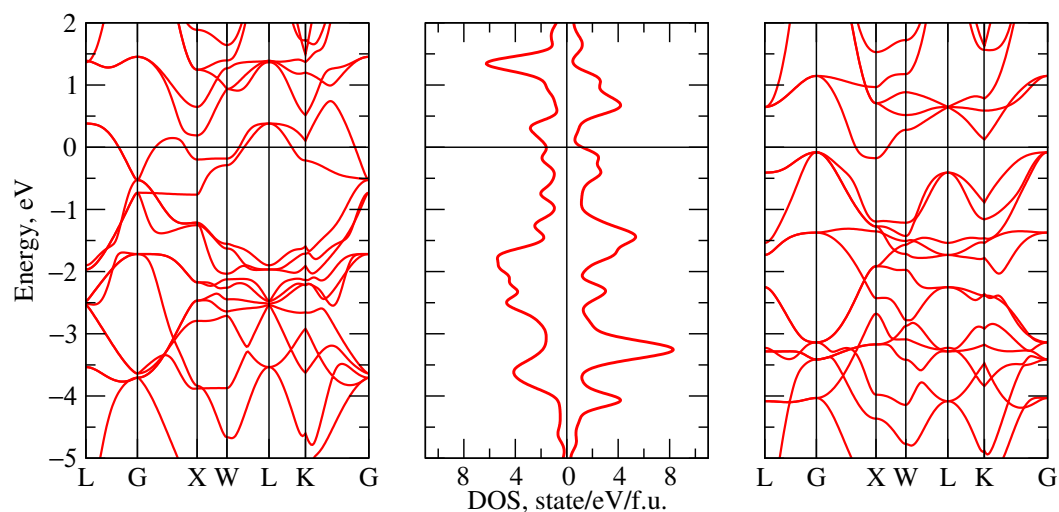


Figure 2. The density of the electronic states and band structure of the compound Mn_2NiAl in the GGA method and lattice parameter $a = 5.795 \text{ \AA}$. The left figure corresponds to band structure of the “minority” spin projection, the mid-figure corresponds to the density of the electronic states, and the right figure corresponds to band structure of the “majority” spin projection. The Fermi energy corresponds to zero energy and is indicated by a horizontal black line.

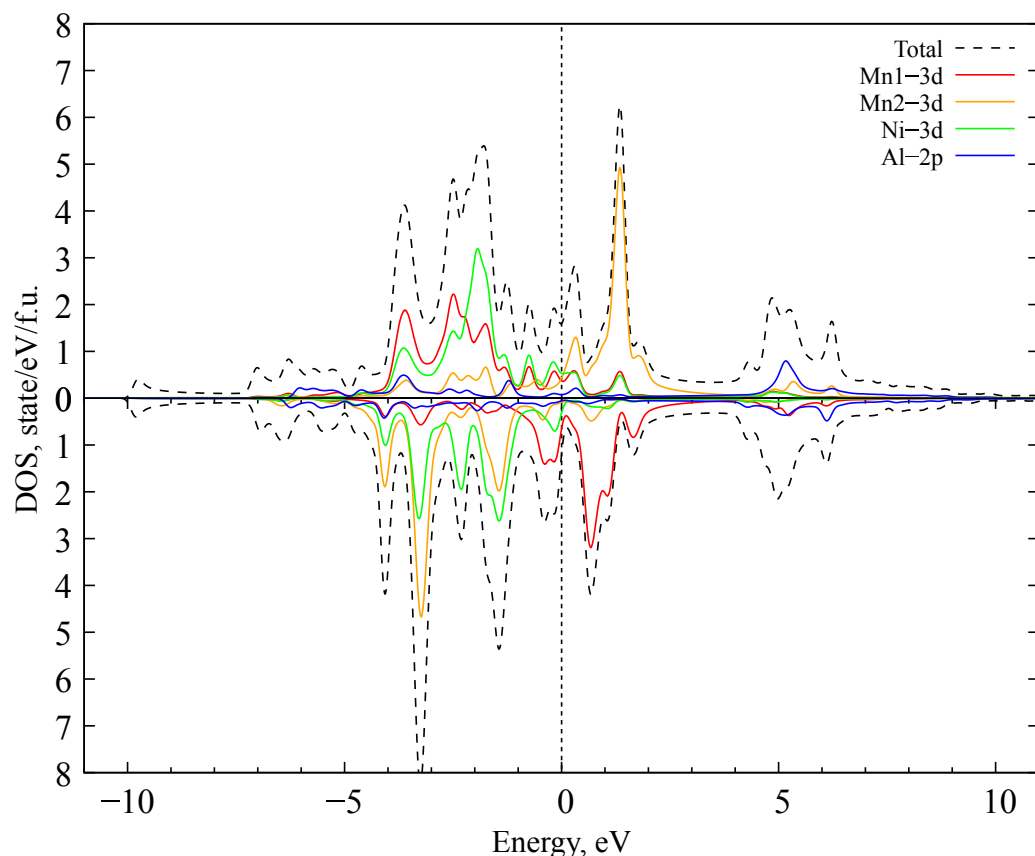


Figure 3. The partial density of the electronic states of Mn_2NiAl in the GGA approximation and lattice parameter $a = 5.795 \text{ \AA}$. The Fermi energy corresponds to zero and is indicated by a vertical dotted line.

Using constrained DFT calculations, we obtain the Coulomb interaction parameter of Mn atoms (3d shell) to be 0.9 eV. In Figure 4, the density of states within the framework of the DFT+U method with $U = 0.9 \text{ eV}$ is presented. With the U parameter included, significant

changes are observed. There is a sliding of 3d states of manganese. The Mn and Ni 3d states are strongly localized, forming three peaks in “majority” and “minority” spin projection. It can be observed that hybridization between the Ni and Mn 3d states both in “minority” spin projection on -1.6 eV and -3.6 eV energy and “majority” spin projection on -2.1 eV and -3.2 eV energy decreases.

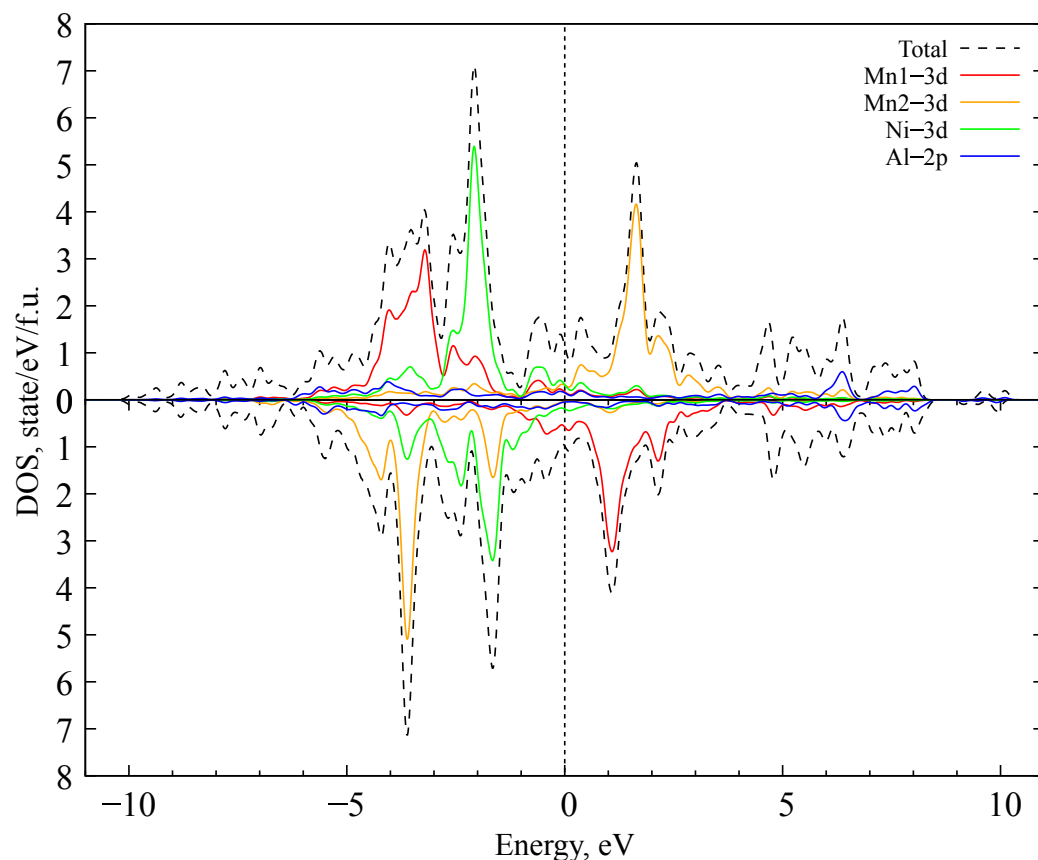


Figure 4. The density of the electronic states of the compound Mn_2NiAl in the framework of the DFT+U method with the Coulomb parameter $U = 0.9$ eV and lattice parameter 5.795 Å. The Fermi level corresponds to zero energy and is indicated by a vertical dotted line.

In Figure 5, the density of states of 3d manganese orbitals are shown more particularly for the Mn1 and Mn2 ions. One can see that both Mn1 and Mn2 have double and triple degenerate e_g and t_{2g} orbitals, respectively. A strong hybridization between xy , zx , zy orbitals and between z^2 and x^2-y^2 is observed. Let us focus on Figure 5a, where the density of states of 3d Mn1 orbitals is shown. A major part of states is localized between -5 and -1.2 eV in the valence band with the “majority” spin projection and from 0 to 2 eV in the conduction band with the “minority” spin projection. The t_{2g} orbitals have several peaks at -4 , -3.2 , and 1.8 eV energy values, the intensity of which reaches 0.8 eV. In case of the e_g orbitals, there are also several peaks localizing in vicinity -3.8 , 1.2, and 2.1 eV. The intensity of these peaks is slightly less and more smeared than the t_{2g} peaks intensity, and reach the value at about 0.7 eV. Also, there are some hybridized states. Let us consider Figure 5b, where the density of states of 3d Mn2 orbitals is shown. A major part of states is localized between the same ranges as in the case of Mn1, but only in the opposite spin projections. The e_g orbitals have two main peaks localizing at -3.8 eV energy in the valence band with the intensity about 1.6 eV, and on 1.8 eV energy in the conduction band with the intensity about 0.6 eV. The t_{2g} orbitals have three pronounced peaks of the density of states. These peaks localize at -4.1 , -1.8 eV energies in the valence band with intensities 0.6 and 0.5 eV, respectively, and at 1.8 eV energy in the conduction band with the intensity about 1.2 eV.

There are also some hybridized states. It is worth noting that the value of peaks intensity of Mn2 is significantly more than the value of peaks intensity of Mn1.

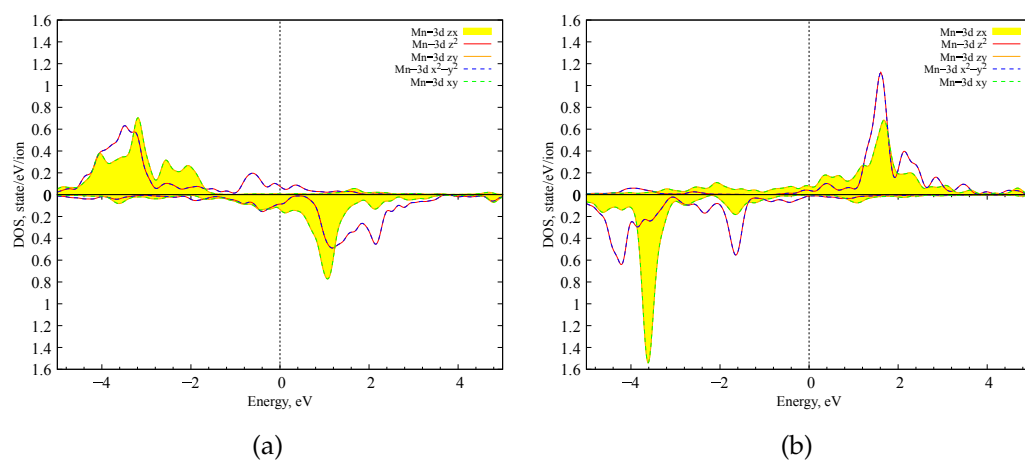


Figure 5. The density of the electronic states of the 3d orbitals of (a) Mn1 (b) Mn2 ions within the DFT+U method with the Coulomb parameter $U = 0.9$ eV. The Fermi level corresponds to zero energy and is indicated by a vertical dotted line.

With the increase of U to 3 eV (Figure 6), the 3d-band become less hybridized Ni and Mn. The Mn 3d states shifted to the low energy levels in the valence band and high energy levels in the conduction band. The Ni 3d states are localized in the vicinity of the -2 eV energy level. In the case of “minority” spin projection, manganese 3d states localize in the valence band in the vicinity of the -5 eV energy level, and in the conduction band in the vicinity of the 1.4 eV energy level. For “majority” spin projection, the same situation is observed except for the fact that the Mn 3d states peak in the conduction band are shifted to the higher energy relative to the Mn 3d states of “majority” spin projection.

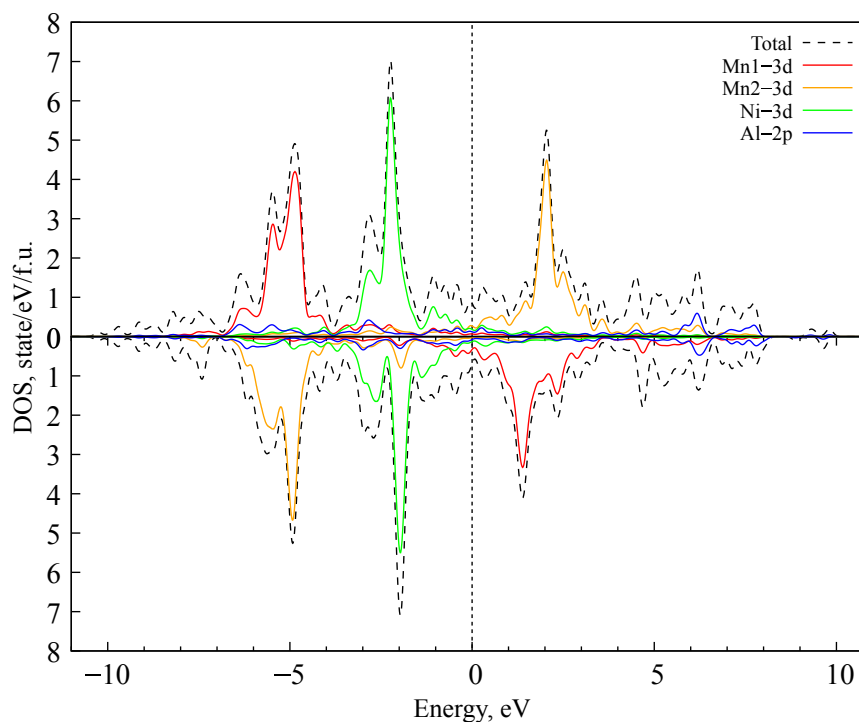


Figure 6. The density of the electronic states of the compound Mn_2NiAl in the framework of the DFT+U method with the Coulomb parameter $U = 3$ eV and lattice parameter 5.795 \AA . The Fermi level corresponds to zero energy and is indicated by a vertical dotted line.

After increasing the Coulomb interaction parameter to 6 eV (Figure 7), a significant displacement of the manganese 3d states to the lower energy is observed in the valence band in each spin projection, but shifting of the manganese 3d states in the conduction band is not obvious and constitutes only 1 eV in the direction of the higher energies. There is also a strict localization of the manganese 3d states. For the Mn1 states, the peaks are localized in the ranges of energies between -8 and -6.75 eV in the valence band and from 1 to 3.5 eV in the conduction band. For the Mn2 states, the peaks are localized in ranges of energies from -8 to -6.5 eV in the valence band and from 2 to 4 eV in the conduction band. It is also worth noting the splitting of the peaks of the 3d states of manganese in the valence band. The Ni 3d states do not shift and localize in the same range of energies between -3.5 and -1 eV in the valence band. Despite these changes, the compound under study retains the metallic properties.

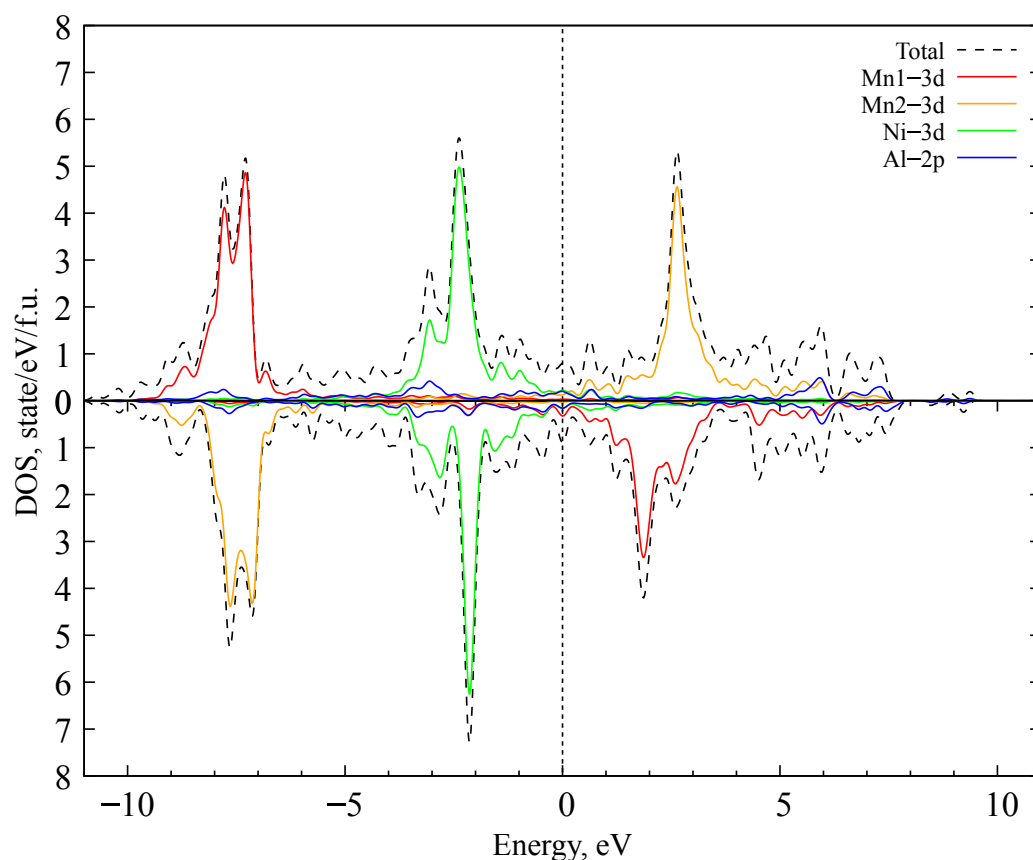


Figure 7. The density of the electronic states of the compound Mn_2NiAl in the framework of the DFT+U method with the Coulomb parameter $U = 6$ eV and lattice parameter 5.795 \AA . The Fermi level corresponds to zero energy and is indicated by a vertical dotted line.

Figure 8 demonstrates the density of the electronic states of the compound Mn_2NiAl in the framework of the HSE method. It can be seen that there are numerous localized maximum peaks throughout the figure, but if we compare the obtained HSE graph with previous DFT+U results, we find that the obtained HSE curve is matched with the DFT+U one for $U = 3$ eV.

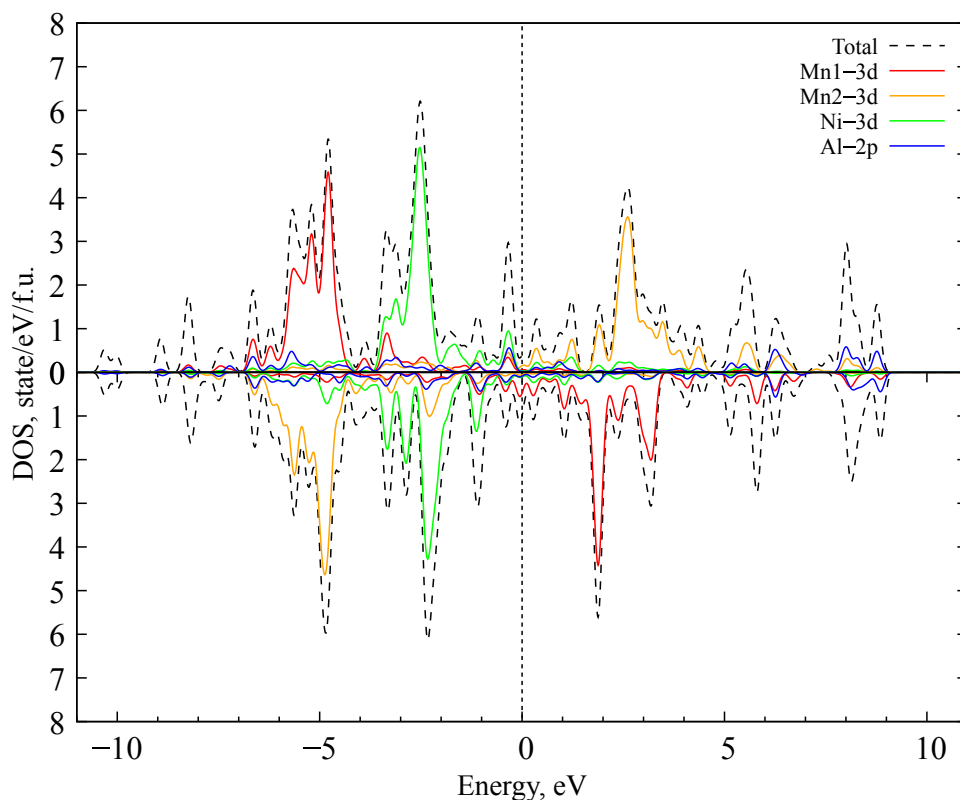


Figure 8. The density of the electronic states of the compound Mn_2NiAl in the framework of the HSE method with lattice parameter 5.795 \AA . The Fermi level corresponds to zero and is indicated by a vertical dotted line.

Let us now focus on Table 1 and Figure 9, where the partial and total magnetic moments are listed. In the case of GGA approximation calculation, the Mn magnetic moments are -2.83 and $3.12 \mu_B$, which correspond to antiparallel ferrimagnetic. The total magnetization is $1.10 \mu_B$ and does not match with experimental value. Considering the Coulomb parameter and using the DFT+U method, Mn magnetic moments become equal to -3.26 and $3.60 \mu_B$ when we include calculated $U = 0.9 \text{ eV}$, which is much more than the case of calculation with the GGA approximation. The total magnetization is reduced by half and equal to $0.54 \mu_B$, which is consistent with the experimental data [20] and in contrast with the previous DFT calculations [17,18]. This decreasing occurs by reduction of the difference between the Mn magnetic moments and reduction of the value of the Ni magnetic moment. When increasing the Coulomb parameter to 3 eV , the difference between Mn magnetic moments continues to decrease. The Mn magnetic moments consist of $-3.75 \mu_B$ and $3.95 \mu_B$ and Ni magnetic moments decrease up to $0.07 \mu_B$, respectively. As a result, the total magnetization reduces to $0.35 \mu_B$. When the Coulomb parameter is 6 eV , the Mn magnetic moments increase up to -4.15 and $4.25 \mu_B$, Ni magnetic moments reduce to $0.00 \mu_B$, and the total magnetization consists of $0.18 \mu_B$. In the case of HSE calculation, the Mn magnetic moments consist of -3.74 and $3.87 \mu_B$, Ni magnetic moments consist of $0.09 \mu_B$, and the total magnetization consists of $0.25 \mu_B$. It also agrees well with the experimental value of total magnetization.

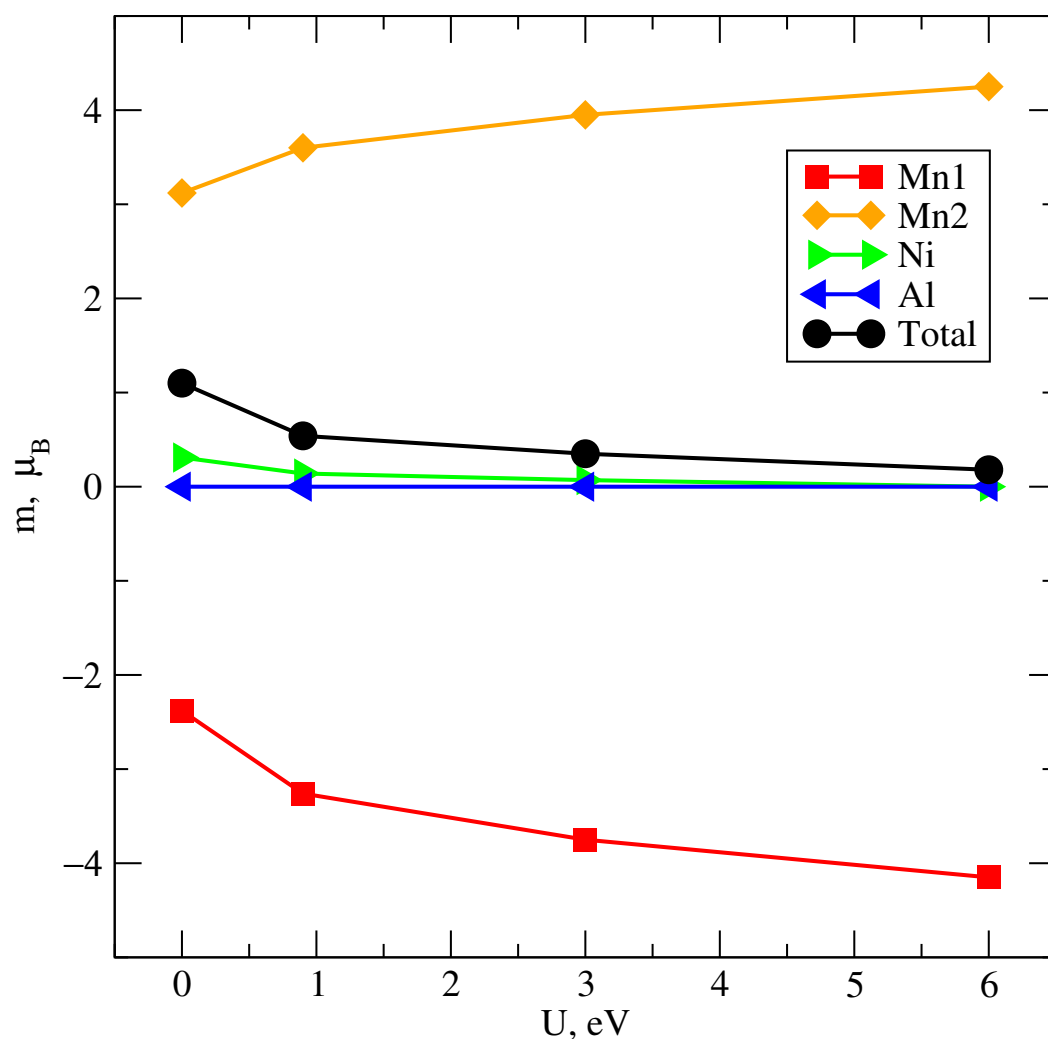


Figure 9. The values of the total and partial per ion magnetic moments for the Mn₂NiAl alloy for different values of the Coulomb interaction parameter. The lattice parameter is 5.795 Å.

Table 1. The values of the magnetic moments of ions in the Mn₂NiAl alloy depend on the value of the Coulomb interaction parameter and the method of calculation. The lattice parameter is 5.795 Å.

U, eV	Mn1, μ _B	Mn2, μ _B	Ni, μ _B	Al, μ _B	Total, μ _B
GGA	−2.38	3.12	0.31	0.00	1.10
0.9	−3.26	3.60	0.14	0.00	0.54
3.0	−3.75	3.95	0.07	0.00	0.35
6.0	−4.15	4.25	0.00	0.00	0.18
HSE	−3.74	3.87	0.09	−0.01	0.25

In our study, we reveal that the experimental lattice parameter does not correspond to the equilibrium minimum total energy of the ground state. Varying the lattice parameter within the range of 5.6 and 6.6 Å, we found that the more energetically favorable lattice parameter is 6.1 Å (Figure 10). Below, we present the results of calculations for Mn₂NiAl with lattice parameter corresponding to 6.1 Å and compare the results obtained.

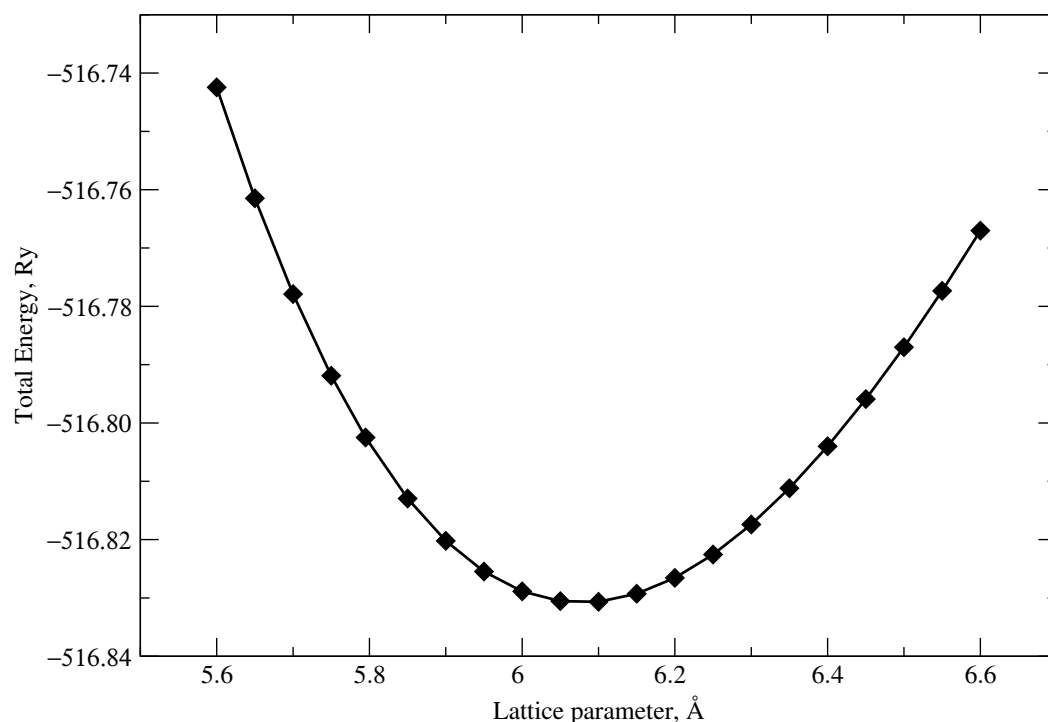


Figure 10. The dependence of the total energy on the lattice parameter.

As in the case of calculation with GGA for Mn_2NiAl with the experimental lattice parameter, let us consider the electronic and band structure of Mn_2NiAl with the energetically favorable lattice parameter in the case of GGA (Figure 11). It can be seen that peaks of density of electronic states on the energy level of -1.5 eV in all spin projections become discernible. This happened as a result of the removal of a strong d-band hybridization between Mn and Ni (Figure 12). In the case of “majority” spin projection, shifting of the 3d-Mn states to the Fermi level is observed. The main peaks of density of Ni 3d states are localized at -1.3 eV and -1.5 eV energy levels in the valence band. The main peaks of the density of Mn1 3d states are localized at the -2.5 eV energy level in the valence band and on 1 eV energy level in the conduction band. The main peaks of density of Mn2 3d states are localized at the -3 eV energy level in the valence band and on 1.75 eV energy level in the conduction band. In general, the type of electronic structure is comparable with the case of the experimental lattice parameter with $U = 0.9$ eV. It is important to note changes in band structure. Now in the case of “minority” spin projection, the Mn band intersects the Fermi level both in the conduction band and the valence band. However, the intersection between the conduction band and the valence band is still not observed. In the case of “majority” spin projection, shifting of the 3d-Mn states to the Fermi level is observed. In spite of this, Mn_2NiAl still exhibits metallic properties.

Similar to the case of the experimental value of the lattice, we calculated the Coulomb interaction parameter using the constrained DFT calculations, and its value is equal to 1 eV. The obtained results are shown in Figure 13. The behavior of Mn_2NiAl with the lattice parameter of 6.1 Å is similar to the behavior of Mn_2NiAl with the lattice parameter of 5.795 Å. There is a decrease in hybridization between 3d states of Ni and Mn. The main peaks of the density of Mn1 3d states localize in the vicinity of the -3.5 eV energy level in the valence band and in the vicinity of the 1.5 eV energy level in the conduction band. In turn, the main peaks of the density of Mn2 3d states localize in the similar range of energy levels in the valence band, but the peak of the density of Mn2 3d states in the conduction band is shifted relative to another peak of the density of Mn1 3d states towards higher energies, and is localized at the 2.3 eV energy level. However, unlike Mn_2NiAl with the lattice parameter of 5.795 eV, the peak of hybridized 3d states of Ni and Mn is observed on

the Fermi level. It is also observed that the weakly intense peaks of 3d-Mn states localize in the vicinity of the Fermi level.

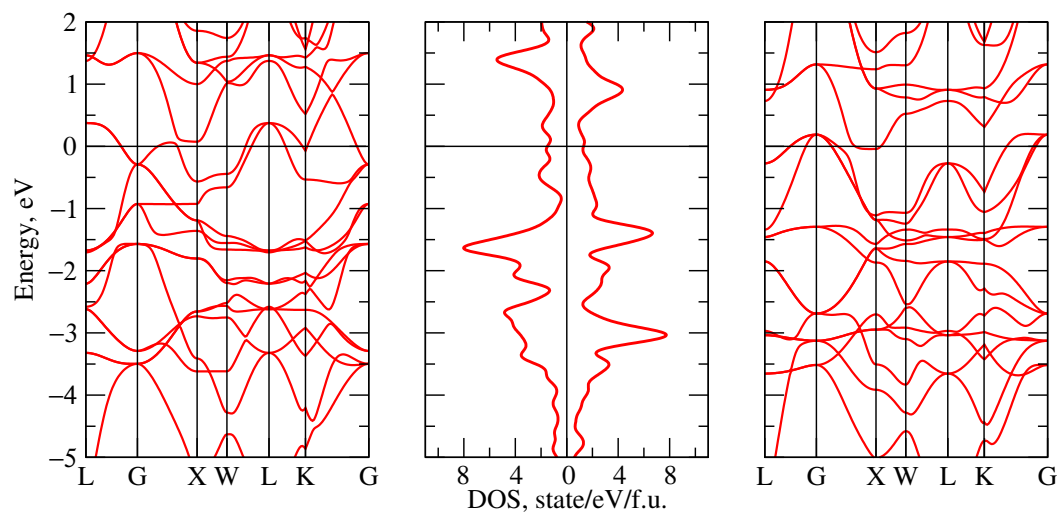


Figure 11. The density of the electronic states and band structure of the compound Mn_2NiAl in the GGA method and lattice parameter $a = 6.1 \text{ \AA}$. The left figure corresponds to band structure of “minority” spin projection, the mid-figure corresponds to the density of the electronic states, and the right figure corresponds to band structure of “majority” spin projection. The Fermi level corresponds to zero energy and is indicated by a horizontal black line.

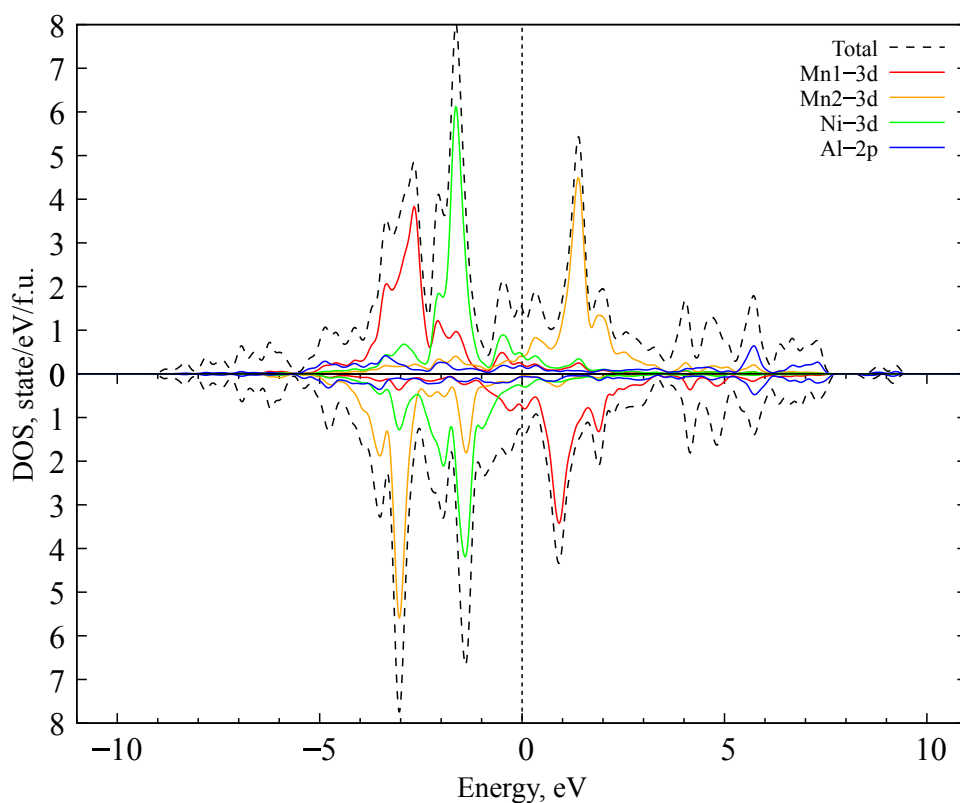


Figure 12. The partial density of the electronic states of the compound Mn_2NiAl in the GGA approximation and lattice parameter $a = 6.1 \text{ \AA}$. The Fermi level corresponds to zero and is indicated by a vertical dotted line.

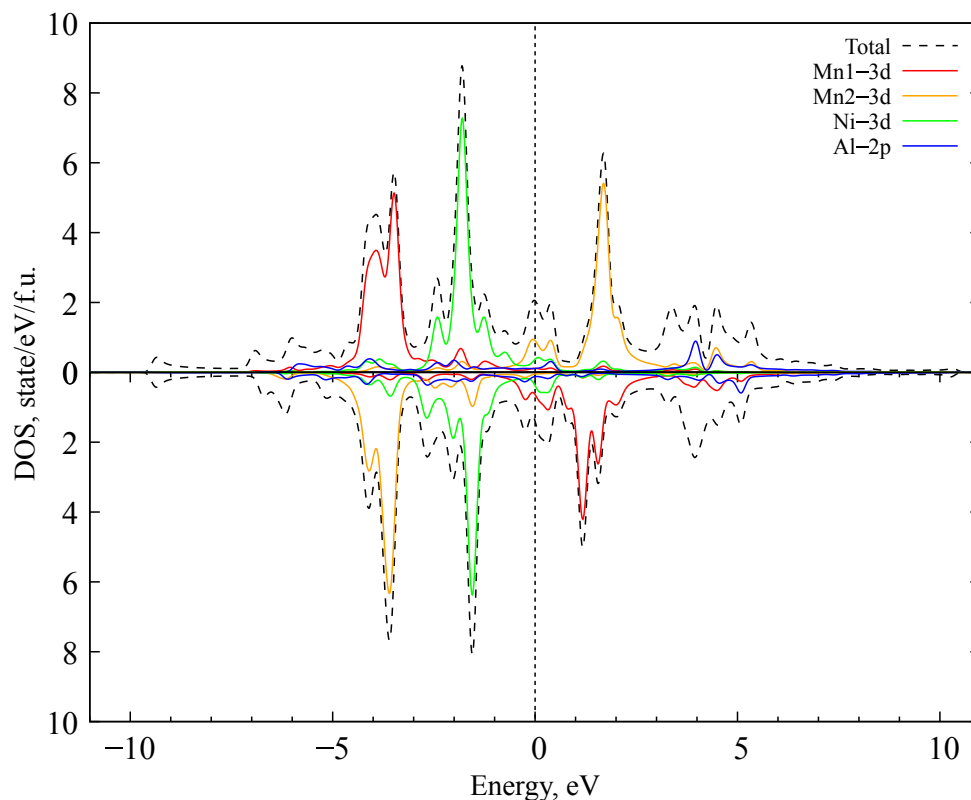


Figure 13. The density of the electronic states of the compound Mn_2NiAl in the framework of the DFT+U method with the Coulomb parameter $U = 1$ eV and lattice parameter of 6.1 \AA . The Fermi level corresponds to zero energy and is indicated by a vertical dotted line.

With the subsequent increase of the Coulomb parameter to 3 eV (Figure 14), a shifting of the electronic states of manganese in proportion to the increase in the Coulomb parameter occurs. However, the main peaks of density of Ni 3d states are localized at the same energy and their intensity does not change. The main peaks of the density of Mn 3d states shift to the -5 eV energy level in the valence band. In the conduction band, there is a shift of 0.25 eV towards high energies, and also the decrease of the intensity of the density of Mn1 3d states occurs. The system under study reacts to a change in the Coulomb parameter in the same way as a system with the experimental value of the lattice constant. The compound under the study retains the metallic properties.

After increasing the Coulomb interaction parameter up to 6 eV (Figure 15), displacement of the manganese 3d states to the lower energy occurs in the valence band in each spin projection. Their intensity increases to 6.2 eV due to localization. There is also a splitting of peaks. The peak of the density of Mn1 3d states in the conduction band splits into two peaks with intensity of about 2.3 eV. The peak of the density of Mn2 3d states shifts to the 3.5 energy level, and its intensity is about 6 eV. It is worth noting that the overall intensity of the peaks decreases due to the removal of hybridization between the 3d states of manganese and nickel. Despite these changes, the compound Mn_2NiAl retains the metallic properties.

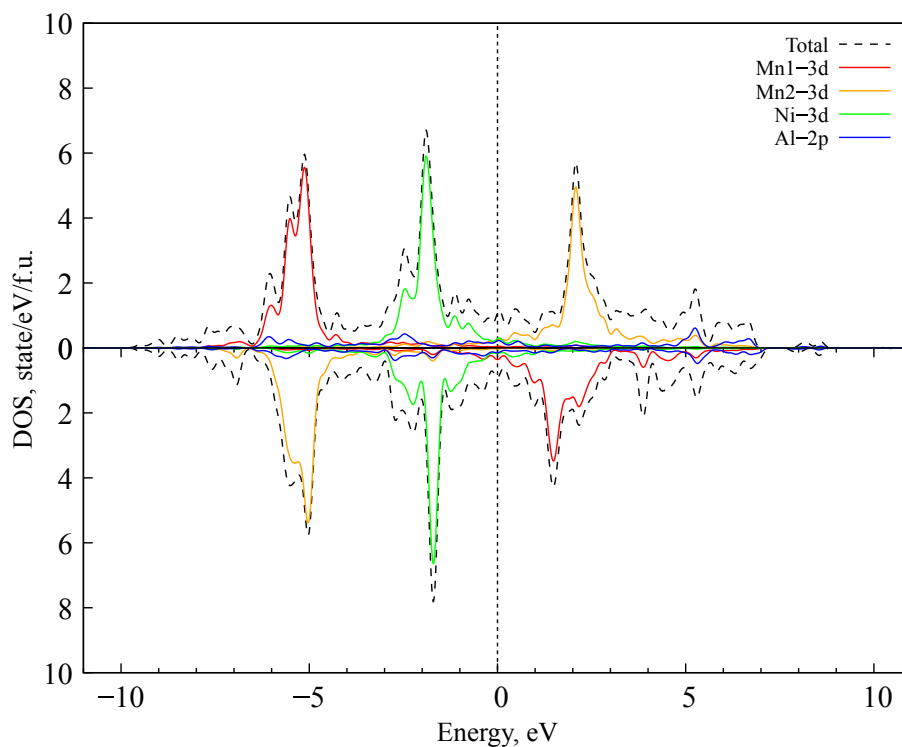


Figure 14. The density of the electronic states of the compound Mn₂NiAl in the framework of the DFT+U method with the Coulomb parameter $U = 3$ eV and lattice parameter of 6.1 Å. The Fermi level corresponds to zero energy and is indicated by a vertical dotted line.

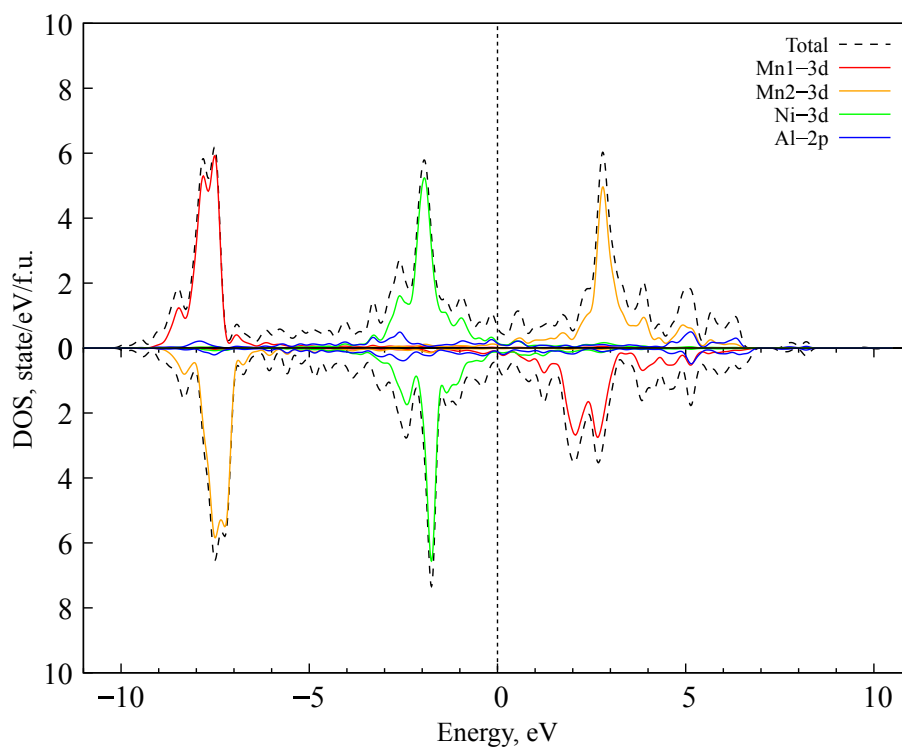


Figure 15. The density of the electronic states of the compound Mn₂NiAl in the framework of the DFT+U method with the Coulomb parameter $U = 6$ eV and lattice parameter of 6.1 Å. The Fermi level corresponds to zero energy and is indicated by a vertical dotted line.

Similar to the HSE calculation presented above for Mn_2NiAl with a lattice constant of 5.795 \AA , a figure of the density of the electronic states of the Mn_2NiAl alloy with a lattice constant of 6.1 \AA was obtained (Figure 16). As can be seen from the figure below, the density of electronic states corresponds to the density of electronic states in the case of DFT+U calculation with the Coulomb parameter of 3 eV .

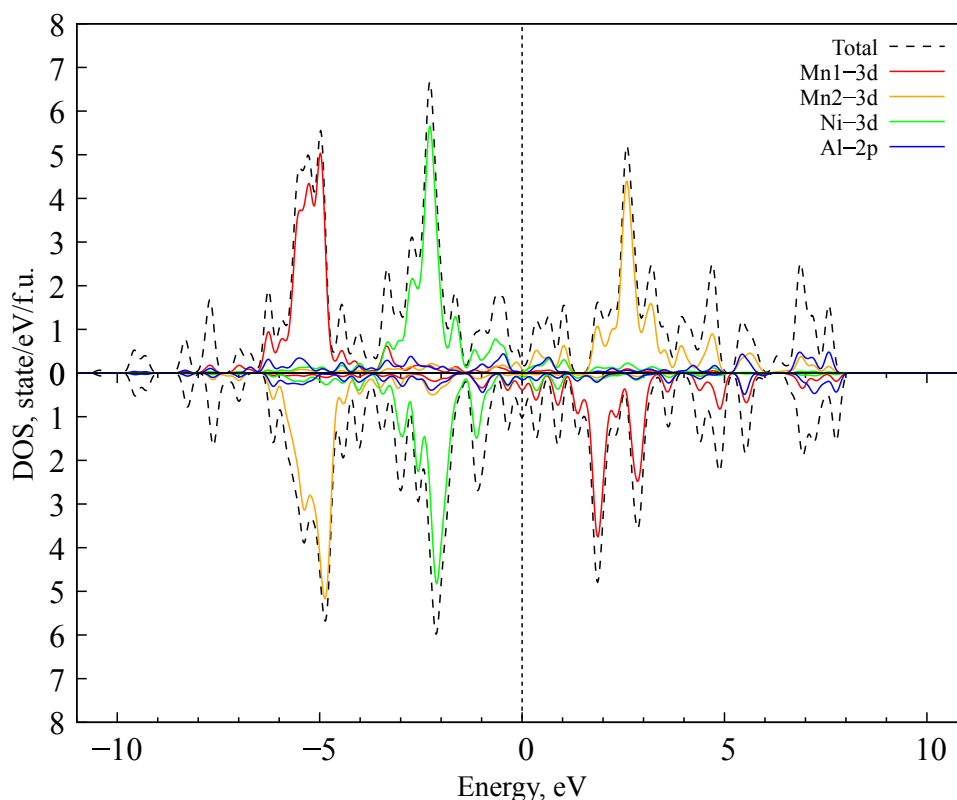


Figure 16. The density of the electronic states of the compound Mn_2NiAl in the framework of the HSE method with lattice parameter of 6.1 \AA . The Fermi level corresponds to zero energy and is indicated by a vertical dotted line.

Unlike the electronic structure, there is a significant change in the magnetic properties (Table 2). The values of the magnetic moments of manganese are noticeably greater (Figure 17). Even when calculated with the GGA approximation, the values of the magnetic moments of manganese are -3.24 and $3.60 \mu_B$, but their change with an increase in the Coulomb parameter remains the same as for Mn_2NiAl with the lattice parameter of 5.795 \AA . With the growth of the Coulomb parameter, the magnetic moments of the manganese increase, reaching -4.43 and $4.46 \mu_B$, respectively, and the difference between them decreases. The behavior of the nickel magnetic moment differs from the previous one. With the growth of the Coulomb parameter, its value decreases, and when the Coulomb parameter reaches 6 eV , the magnetic moment of nickel changes its orientation and takes the value $-0.04 \mu_B$. The total magnetization of the unit cell at the lattice parameter of 6.1 \AA is slightly lower. Without taking into account the Coulomb parameter, its value is $0.59 \mu_B$. With an increase in the Coulomb parameter, the total magnetization decreases, reaching a value of $0.02 \mu_B$. In the case of the HSE calculation, the obtained values of the total magnetization agree well with the experimental data [20].

Table 2. The values of the magnetic moments of ions in the Mn_2NiAl compound depend on the value of the Coulomb interaction parameter and the method of calculation. The lattice parameter is 6.1 Å.

U, eV	Mn1, μ_B	Mn2, μ_B	Ni, μ_B	Al, μ_B	Total, μ_B
GGA	−3.24	3.60	0.18	0.00	0.59
1.0	−3.78	3.97	0.07	0.00	0.32
3.0	−4.12	4.23	0.01	0.00	0.19
6.0	−4.43	4.46	−0.04	0.00	0.02
HSE	−4.08	4.14	0.04	0.00	0.14

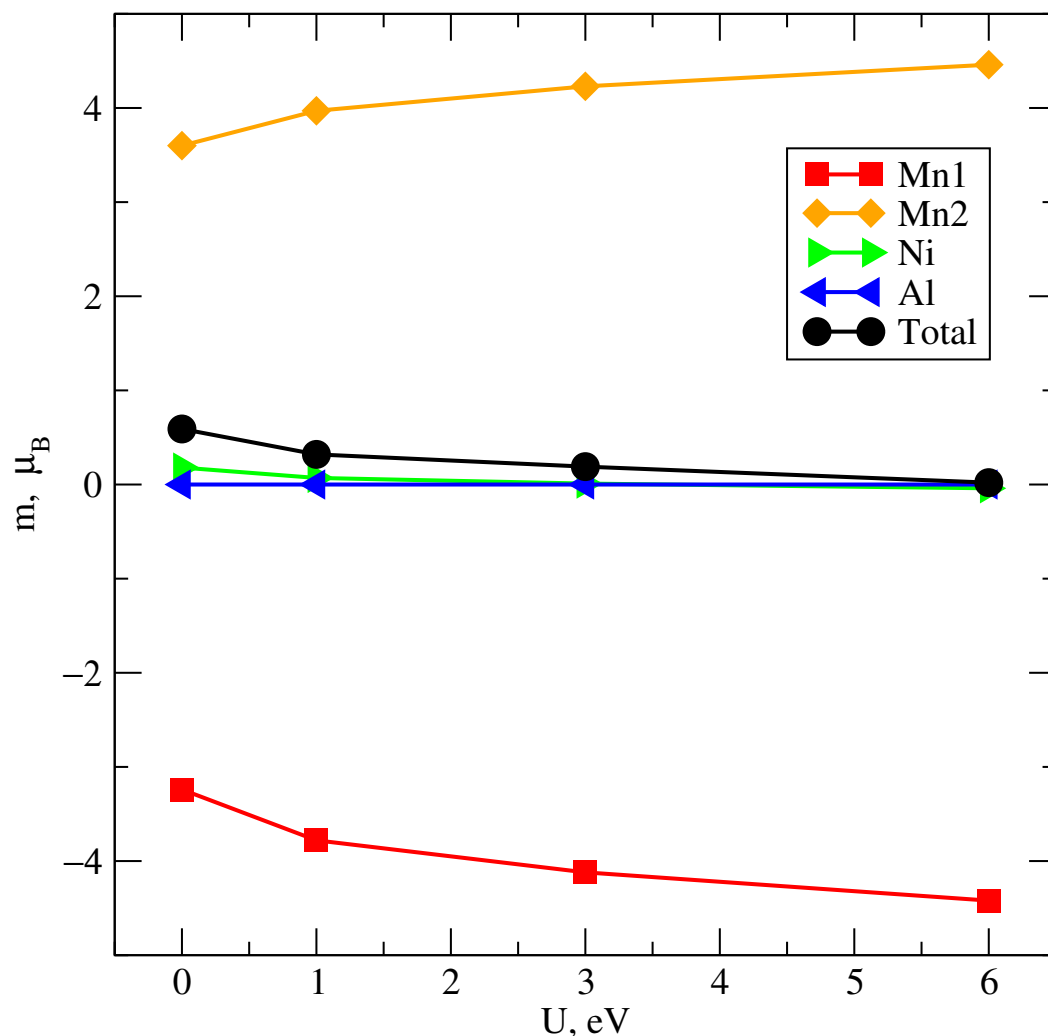


Figure 17. The total and partial per ion magnetic moments for the Mn_2NiAl alloy for different values of the Coulomb interaction parameter. The lattice parameter is 6.1 Å.

4. Conclusions

In our theoretical study, the electronic structures of Mn_2NiAl were investigated within the framework of DFT+U and HSE and found to be metallic in all calculations. The dependence of the magnetic moments of the ions and total magnetic moment on the Coulomb parameter was revealed. The equilibrium lattice parameter value was obtained as 6.10 Å; for this reason, we analyzed both experimental and equilibrium lattice parameters in the work. It was shown that the U values taken into account, including the one calculated in the constrained LDA approach, result in changes of both the magnetic moments and electronic structure of the Heusler alloy under study. The dependence of the total and partial magnetic moments on the U value was revealed and plotted. The total magnetic

moments are in good agreement with the experimental magnetization of $0.19 \mu_B$ [20] for the moderate values of the Coulomb parameter in the case of the equilibrium lattice parameter. The HSE calculations for Mn_2NiAl also resulted in the close magnetic moment values for both experimental and calculated lattice parameters. The results obtained suggest that it is necessary to take into account electron correlations in this alloy.

Author Contributions: Conceptualization, A.V.L.; methodology, E.D.C. and A.V.L.; software, E.D.C.; validation, A.V.L.; investigation, E.D.C.; writing—original draft preparation, E.D.C.; writing—review and editing, A.V.L.; supervision, A.V.L.; project administration, A.V.L. All authors have read and agreed to the published version of the manuscript.

Funding: The research was supported by the Russian Science Foundation, project no. 22-22-20109 (<https://rscf.ru/en/project/22-22-20109/>), M.N. Mikheev Institute of Metal Physics of Ural Branch of Russian Academy of Sciences).

Institutional Review Board Statement: Not applicable.

Informed Consent Statement: Not applicable.

Data Availability Statement: The data presented in this study are available on request from the corresponding author.

Conflicts of Interest: The authors declare no conflict of interest. The funders had no role in the design of the study; in the collection, analyses, or interpretation of data; in the writing of the manuscript, or in the decision to publish the results.

References

1. Graf, T.; Felser, C.; Parkin, S.S.P. Simple rules for the understanding of Heusler compounds. *Prog. Solid. State Chem.* **2011**, *1*, 1–50. [[CrossRef](#)]
2. Sanvito, S.; Oses, C.; Xue, J.; Tiwari, A.; Zic, M.; Archer, T.; Tozman, P.; Venkatesan, M.; Coey, M.; Curtarolo, S. Accelerated discovery of new magnets in the Heusler alloy family. *Sci. Adv.* **2017**, *4*, e1602241. [[CrossRef](#)]
3. Al-Masri, K.M.; Abu-Jafar, M.S.; Farout, M.; Dahliah, D.; Mousa, A.A.; Azar, S.M.; Khenata, R. Structural, Elastic, Electronic, and Magnetic Properties of Full-Heusler Alloys Sc_2TiAl and Sc_2TiSi Using the FP-LAPW Method. *Magnetochemistry* **2023**, *9*, 108. [[CrossRef](#)]
4. Ohno, H. Making Nonmagnetic Semiconductors Ferromagnetic. *Science* **1998**, *281*, 951–956. [[CrossRef](#)]
5. Graf, T.; Felser, C.; Parkin, S.S.P. Heusler Compounds: Applications in Spintronics. In *Handbook of Spintronics*; Xu, Y., Awschalom, D., Nitta, J., Eds.; Springer: Dordrecht, The Netherlands, 2016. [[CrossRef](#)]
6. Patel, A.K.; Samatham, S.S.; Lukoyanov, A.V.; Babu, P.D.; Suresh, K.G. Nearly compensated ferrimagnetic behaviour and giant exchange bias of hexagonal Mn_2PtAl : experimental and theoretical studies. *Phys. Chem. Chem. Phys.* **2022**, *24*, 29539–29546. [[CrossRef](#)]
7. Balke, B.; Fecher, G.H.; Kandpal, H.C.; Felser, C.; Kobayashi, K.; Ikenaga, E.; Kim, J.J.; Ueda, S. Properties of the quaternary half-metal-type Heusler alloy $Co_2Mn_{1-x}Fe_xSi$. *Phys. Rev. B* **2006**, *74*, 104405. [[CrossRef](#)]
8. Dash, S.; Lukoyanov, A.V.; Mishra, D.; Rasi, U.M.; Gangineni, R.B.; Vasundhara, M.; Patra, A.K. Structural stability and magnetic properties of Mn_2FeAl alloy with a β -Mn structure. *J. Magn. Magn. Mater.* **2020**, *513*, 167205. [[CrossRef](#)]
9. Şaşıoğlu, E.; Galanakis, I.; Friedrich, C.; Blügel, S. Ab initio calculation of the effective on-site Coulomb interaction parameters for half-metallic magnets. *Phys. Rev. B* **2013**, *88*, 134402. [[CrossRef](#)]
10. Kandpal, H.C.; Fecher, G.H.; Felser, C.; Schönhense, G. Correlation in the transition-metal-based Heusler compounds Co_2MnSi and Co_2FeSi . *Phys. Rev. B* **2006**, *73*, 094422. [[CrossRef](#)]
11. Tas, M.; Şaşıoğlu, E.; Blügel, S.; Mertig, I.; Galanakis, I. Ab initio calculation of the Hubbard U and Hund exchange J in local moment magnets: The case of Mn-based full Heusler compounds. *Phys. Rev. Mater.* **2022**, *6*, 114401. [[CrossRef](#)]
12. Liu, G.D.; Chen, J.L.; Liu, Z.H.; Dai, X.F.; Wu, G.H.; Zhang, B.; Zhang, X.X. Martensitic transformation and shape memory effect in a ferromagnetic shape memory alloy: Mn_2NiGa . *Appl. Phys. Lett.* **2005**, *26*, 262504. [[CrossRef](#)]
13. Lakshmi, N.; Pandey, A.; Venugopalan, K. Hyperfine field distributions in disordered Mn_2CoSn and Mn_2NiSn Heusler alloys. *Bull. Mater. Sci.* **2002**, *25*, 309–313. [[CrossRef](#)]
14. Kervan, N.; Kervan, S.; Canko, O.; Osman Canko, O.; Atiş, M.; Taşkın, F. Half-Metallic Ferrimagnetism in the Mn_2NbAl Full-Heusler Compound: a First-Principles Study. *J. Supercond. Nov. Magn.* **2016**, *29*, 187–192. [[CrossRef](#)]
15. Masrour, R.; Jabbar, A.; Labidi, S.; El Krimi, Y.; Ellouze, M.; Labidi, M.; Amara, A. Study of structural, elastic, thermal, electronic and magnetic properties of heusler Mn_2NiGe : An Ab initio calculations and Monte Carlo simulations. *Mater. Today Commun.* **2021**, *26*, 101772. [[CrossRef](#)]
16. Li, X. Z.; Zhang, W. Y.; Sellmyer, D. J. Structural investigation of phase segregation in Mn_2CrGa -based alloys. *Acta Mater.* **2017**, *140*, 188–195. [[CrossRef](#)]

17. Luo, H.; Liu, G.; Meng, F.; Li, S.; Zhu, W.; Wu, G.; Jiang, C. Electronic structure and magnetism of the Heusler alloy Mn₂NiAl: A theoretical study of the shape–memory behavior. *Phys. B Condens. Matter* **2010**, *15*, 3092–3095. [[CrossRef](#)]
18. Luo, L.J.; Zhong, C.G.; Fang, J.H.; Zhou, P.X.; Zhao, Y.L.; Jiang, X.F. First-principles study of electronic and magnetic properties and tetragonal distortion of the Heusler alloy Mn₂NiAl. *J. At. Mol. Sci.* **2011**, *2*, 368–376. [[CrossRef](#)]
19. Zhao, R.B.; Zhao, D.W.; Li, G.K.; Ma, L.; Zhen, C.M.; Hou, D.L.; Wu, G.H. Anomalous magnetic configuration of Mn₂NiAl ribbon and the role of hybridization in the martensitic transformation of Mn₅₀Ni_{50-x}Al_x ribbons. *Appl. Phys. Lett.* **2014**, *23*, 232404. [[CrossRef](#)]
20. Marchenkov, V.V.; Irkhin, V.Y.; Perevozchikova, Y.A.; Terent'ev, P.B.; Semiannikova, A.A.; Marchenkova, E.B.; Eisterer, M. Kinetic Properties and Half-Metallic Magnetism in Mn₂YAl Heusler Alloys. *J. Exp. Theor. Phys.* **2019**, *128*, 919–925. [[CrossRef](#)]
21. Momma, K.; Izumi, F. VESTA 3 for three-dimensional visualization of crystal, volumetric and morphology data. *J. Appl. Crystallogr.* **2011**, *44*, 1272–1276. [[CrossRef](#)]
22. Giannozzi, P.; Andreussi, O.; Brumme, T.; Bunau, O.; Buongiorno Nardelli, M.; Calandra, M.; Car, R.; Cavazzoni, C.; Ceresoli, D.; Cococcioni, M.; et al. Advanced capabilities for materials modelling with Quantum ESPRESSO. *J. Phys. Condens. Matter* **2017**, *29*, 465901. [[CrossRef](#)] [[PubMed](#)]
23. Perdew, J.P.; Burke, K.; Ernzerhof, M. Generalized gradient approximation made simple. *Phys. Rev. Lett.* **1996**, *77*, 3865–3868. [[CrossRef](#)] [[PubMed](#)]
24. Anisimov, V.I.; Gunnarsson, O. Density-Functional Calculation of Effective Coulomb Interactions in Metals. *Phys. Rev. B* **1991**, *43*, 7570–7574. [[CrossRef](#)] [[PubMed](#)]
25. Quantum ESPRESSO. Available online: <https://www.quantum-espresso.org/pseudopotentials> (accessed on 4 June 2023).

Disclaimer/Publisher's Note: The statements, opinions and data contained in all publications are solely those of the individual author(s) and contributor(s) and not of MDPI and/or the editor(s). MDPI and/or the editor(s) disclaim responsibility for any injury to people or property resulting from any ideas, methods, instructions or products referred to in the content.